JCB Journal of Cell Biology

REPORT

Wnts regulate planar cell polarity via heterotrimeric G protein and PI3K signaling

Andre Landin Malt[1], Arielle K. Hogan[1], Connor D. Smith[1], Maxwell S. Madani[1], and Xiaowei Lu[1]

In the mammalian cochlea, the planar cell polarity (PCP) pathway aligns hair cell orientation along the plane of the sensory epithelium. Concurrently, multiple cell intrinsic planar polarity (referred to as iPCP) modules mediate planar polarization of the hair cell apical cytoskeleton, including the kinocilium and the V-shaped hair bundle essential for mechanotransduction. How PCP and iPCP are coordinated during development and the roles of Wnt ligands in this process remain unresolved. Here we show that genetic blockade of Wnt secretion in the cochlear epithelium resulted in a shortened cochlear duct and misoriented and misshapen hair bundles. Mechanistically, Wnts stimulate Gi activity by regulating the localization of Daple, a guanine nucleotide exchange factor (GEF) for Gαi. In turn, the Gβγ complex signals through phosphoinositide 3-kinase (PI3K) to regulate kinocilium positioning and asymmetric localizations of a subset of core PCP proteins, thereby coordinating PCP and iPCP. Thus, our results identify a putative Wnt/heterotrimeric G protein/PI3K pathway for PCP regulation.

Introduction

The vertebrate PCP pathway mediates a noncanonical, β-catenin–independent Wnt signaling cascade and regulates a plethora of developmental processes (Butler and Wallingford, 2017). Mammalian "core" PCP proteins include orthologues of *Drosophila melanogaster* Frizzled (Fzd3/6), Dishevelled (Dvl1-3), Van Gogh (Vangl1/2), Flamingo (Celsr1-3), Prickle (Pk1-2), and Diego (Ankrd6). Core PCP proteins orient cell polarity along a tissue plane by forming two polarized protein complexes that interact across intercellular junctions and generate cytoskeletal asymmetry through Rho family GTPases. While Wnt ligands are involved in PCP regulation in vertebrates, the underlying mechanisms are poorly understood (Aw and Devenport, 2017; Yang and Mlodzik, 2015).

Accumulating evidence suggests that heterotrimeric G proteins are involved in noncanonical Wnt signaling (Nichols et al., 2013; Schulte and Wright, 2018). Classical G protein–coupled receptors (GPCRs) stimulate exchange of GTP for GDP on the Gα subunit, triggering its dissociation from the Gβγ heterodimer. Subsequently, Gβγ and Gα-GTP can separately activate distinct downstream effectors (Oldham and Hamm, 2008). Although Frizzled receptors are a class of GPCRs, it is debated whether they can directly activate G proteins. Cell culture experiments demonstrated that Wnt5a-activated Fzd7 can induce G protein signaling not as a classic GPCR, but by binding to the nonreceptor guanine nucleotide exchange factor (GEF) Daple/Ccdc88c (Aznar et al., 2015). Daple can also bind the PSD-95/DLG/ZO1 (PDZ) domain of Dishevelled and activate noncanonical Wnt signaling (Ishida-Takagishi et al., 2012). Thus, Wnt/G protein signaling may be mechanistically and functionally linked to the PCP pathway. However, the roles of Wnt/G protein signaling in mammalian tissue morphogenesis, particularly in PCP regulation, remain unknown.

Auditory hair cells (HCs) in the organ of Corti (OC) manifest hallmark features of PCP (Tarchini and Lu, 2019). Essential for their function as sound receptors, individual HCs assemble a hair bundle on their apical surface consisting of rows of actin-based stereocilia arranged in a staircase pattern. Hair bundle formation is initiated by the centrifugal migration of the HC primary cilium, the kinocilium, toward the lateral pole of the HC. Surrounding microvilli then elongate into stereocilia, which interconnect to form a V-shaped hair bundle with the kinocilium tethered at the vertex. Thus, the asymmetric apical cytoskeleton defines HC intrinsic planar polarity, or iPCP (Fig. 1 a'). Concurrent with iPCP establishment, HCs become uniformly oriented along the medial-lateral axis of the cochlear duct, which defines tissue-level PCP (Fig. 1 a).

The PCP pathway mediates intercellular signaling between HCs and neighboring supporting cells (SCs) to align iPCP. Core PCP proteins are planar polarized on the medial-lateral HC-SC apical junctions (Etheridge et al., 2008; Montcouquiol et al., 2006; Wang et al., 2005, 2006). PCP mutants have misoriented hair bundles and a shortened cochlear duct due to

[1]Department of Cell Biology, University of Virginia Health System, Charlottesville, VA.

Correspondence to Xiaowei Lu: xl6f@virginia.edu.

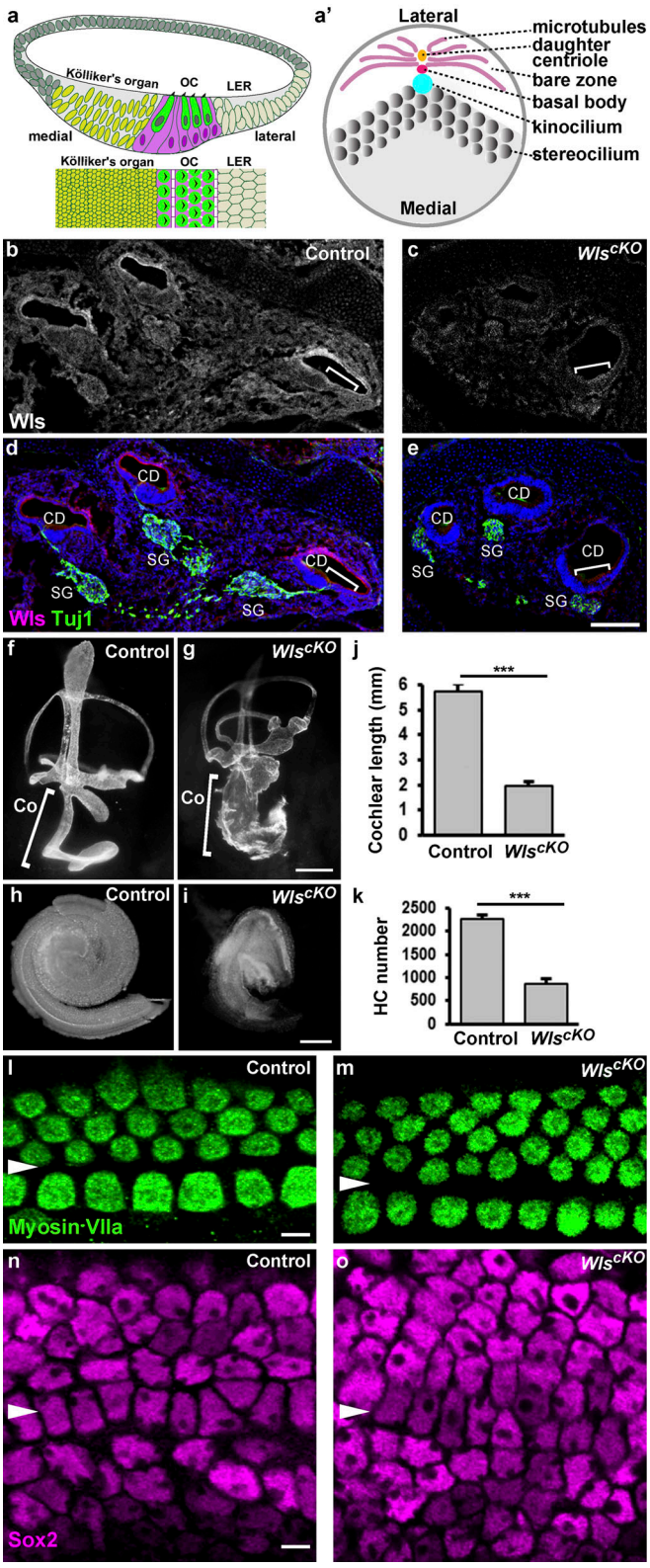

Figure 1. **Growth defects in *Wls*^{cKO} cochleae. (a)** Schematic diagrams of a cochlear duct (CD) cross-section (top), and en face view of the OC and surrounding nonsensory epithelia (bottom). HCs are colored green and SCs magenta. **(a')** A schematic diagram of the HC apical cytoskeleton. The medially polarized microvilli zone is shown in gray. **(b–e)** Cross-sections of E16.5 control (b and d) and *Wls*^{cKO} cochleae (c and e) stained for Wls (magenta), Tuj1 (green), and nuclei (blue). **(f and g)** Paint-filled control (f) and *Wls*^{cKO} (g) inner ears at E14.5. **(h and i)** Dissected E18.5 control (h) and *Wls*^{cKO} cochleae (i). **(j and k)** Quantifications of cochlear length and HC numbers. *n* = 6 for each genotype. ***, P < 0.001. **(l–o)** Confocal images of E18.5 control (l and n) and *Wls*^{cKO} OC (m and o) stained for myosin VIIa and Sox2. Arrowheads indicate the pillar cell row. Scale bars: b–e, 100 µm; f and g, 250 µm; h and i, 100 µm; l–o, 6 µm. Co, cochlea; LER, lesser epithelial ridge; SG, spiral ganglion.

defective cochlear extension. PCP signaling is dispensable for iPCP establishment. Distinct from PCP defects, mutants for iPCP effectors had misshapen hair bundles with the kinocilium detached or positioned "off-center" in relation to the midpoint of the hair bundle, often accompanied by hair bundle misorientation. Several planar polarized iPCP effector modules including Rac1 and Cdc42 GTPases, cell polarity proteins, and microtubule motors act in concert to couple hair bundle orientation with kinocilium positioning (Ezan et al., 2013; Grimsley-Myers et al., 2009; Kirjavainen et al., 2015; Landin Malt et al., 2019; Siletti et al., 2017; Sipe et al., 2013; Sipe and Lu, 2011; Tarchini et al., 2013). Of particular interest, Gαi proteins and their regulators LGN/G protein signaling modulator 2 (Gpsm2) and Daple are essential for iPCP in the OC (Beer-Hammer et al., 2018; Ezan et al., 2013; Siletti et al., 2017; Tarchini et al., 2013). Here, we investigate the unsolved questions regarding the function of heterotrimeric G protein signaling and its regulation by Wnts during PCP establishment in the OC.

Results and discussion

Epithelial Wnts are required for cochlear outgrowth

Published RNA-sequencing data have shown that many Wnt ligands are expressed in the developing mouse cochlea at embryonic day (E)16, when both iPCP and PCP signaling are active (Scheffer et al., 2015). To localize the source of secreted Wnt ligands, we examined the distribution of Wntless (Wls)/GPR177, a transmembrane protein required for secretion of all Wnt ligands (Bänziger et al., 2006; Bartscherer et al., 2006). At E16.5, Wls is highly enriched on the luminal surface of the cochlear duct, including the OC and adjacent nonsensory epithelia (Fig. 1, b and d, brackets). Wls is also expressed in the otic mesenchyme and the spiral ganglion. To determine the function of epithelial Wnts in cochlear morphogenesis, we generated a conditional knockout of Wls (*Wls*^{cKO}) by deleting *Wls* in the developing cochlear epithelium. At E16.5, Wls expression was significantly reduced in the *Wls*^{cKO} cochlear duct, confirming Wls deletion (Fig. 1, c and e). No live *Wls*^{cKO} pups were recovered, and E18.5 *Wls*^{cKO} embryos displayed developmental defects in multiple organs, consistent with the Cre expression patterns (Fig. S1). The *Wls*^{cKO} cochlear duct was significantly shorter and dilated at E14.5 (Fig. 1, f and g, brackets). By E18.5, the length of the *Wls*^{cKO} cochlea was about one third of the normal length (Fig. 1, h–j). We next assessed HC and SC specification using the HC marker Myosin VIIa and SC marker Sox2. Myosin VIIa expression in HCs and Sox2 expression in SCs was comparable between the control and *Wls*^{cKO} cochlea (Fig. 1, l–o). However, HC numbers were greatly reduced in *Wls*^{cKO} OC, and extra rows of outer HCs and SCs were frequently observed toward the cochlear apex (Fig. 1, k–o). Thus, cell fate specification in the OC

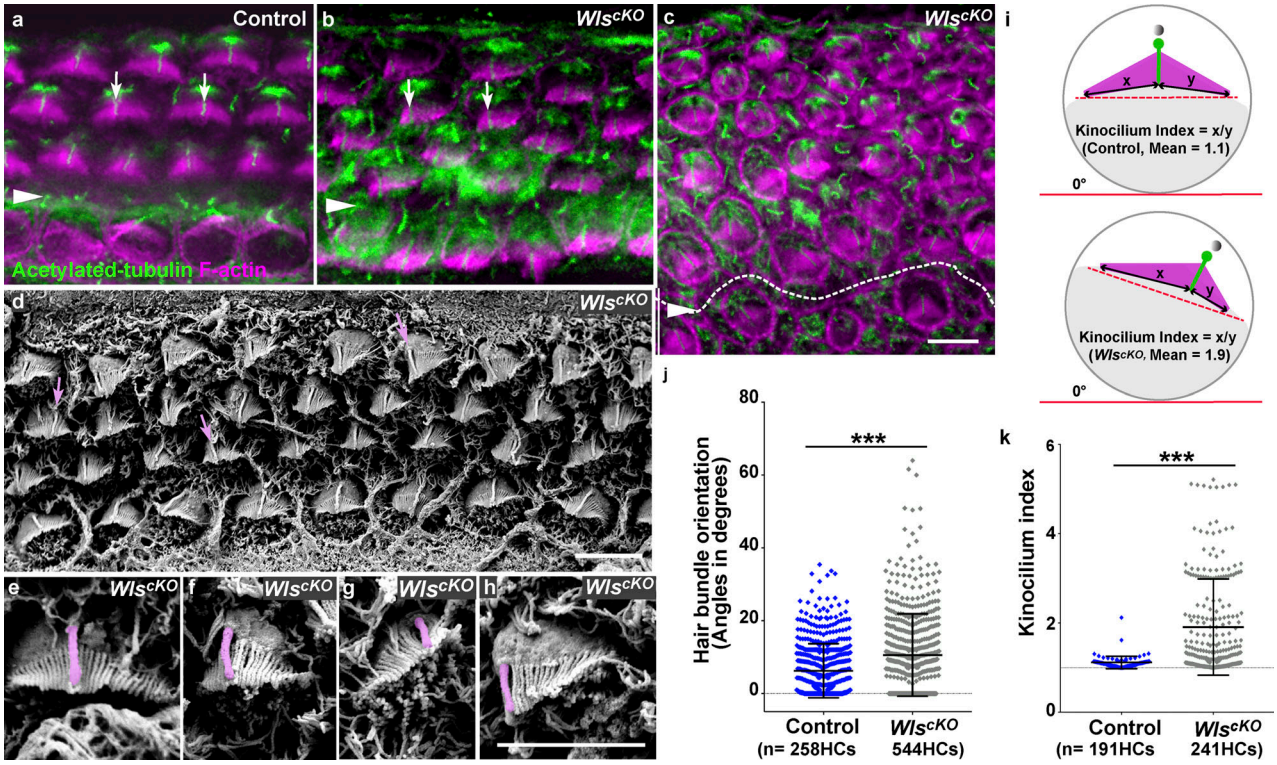

Figure 2. **Hair bundle orientation and kinocilium positioning defects in *Wls*^{cKO} cochleae. (a–c)** E18.5 control (a) and *Wls*^{cKO} OC (b and c) stained for acetylated tubulin (labeling the kinocilium, green) and F-actin (labeling the hair bundle, magenta). **(d–h)** Scanning electron micrographs of *Wls*^{cKO} hair bundles. Kinocilia are indicated by arrows (a, b, and d) or pseudo-colored (e–h). **(i)** Schematic diagrams for measurements of hair bundle orientation and kinocilium positioning. **(j and k)** Quantifications of hair bundle orientation (j) and kinocilium positioning (k). ***, P < 0.001. Scale bars: a–c, 6 µm; d–h, 4 µm.

can proceed independently of epithelial Wnt ligands, but Wnts are required for normal cochlear outgrowth and HC numbers.

PCP and iPCP defects in the *Wls*^{cKO} OC

To assess HC polarity, we next examined hair bundle morphogenesis. At E18.5, both iPCP and PCP were evident in control HCs: the kinocilium was positioned at the hair bundle vertex and near the lateral pole of HCs (Fig. 2 a and Fig. S1 h). In contrast, many *Wls*^{cKO} HCs had misoriented and misshapen hair bundles with an off-center kinocilium (Fig. 2, b–k; and Fig. S1 i), indicating defects in both PCP and iPCP. Hair bundle misorientation was more severe toward the apex, where outer hair cell (OHC) rows were disorganized (Fig. 2 c). Of note, kinocilium migration, an early step in iPCP, was not affected in *Wls*^{cKO} HCs. Together, the hair bundle shape and orientation defects indicate that Wnt signaling regulates both iPCP and PCP in the OC.

In *Wls*^{cKO} OC, hair bundle misorientation was mild compared to PCP null mutants (Montcouquiol et al., 2003; Song et al., 2010), suggesting a partial impairment of PCP signaling. To pinpoint the role of secreted Wnts in PCP signaling, we examined the localization of representative core PCP proteins. At E18.5, Fzd6 was enriched along the medial junctions and Dvl2 along the lateral junctions of HCs in the control (Fig. 3, a, b, e, and f, arrows; and Fig. 3 s). In *Wls*^{cKO} OC, junctional localization of Fzd6 was greatly reduced (Fig. 3, c, d, and s); and similarly, Dvl2 was delocalized from lateral HC junctions and distributed diffusely in SC phalangeal processes (Fig. 3, g, h, and s). By contrast, asymmetric localization of Vangl2 along the medial HC junctions was largely intact (Fig. 3, i–l, arrows; Fig. 3 s). Likewise, Dvl3 was enriched along the medial-lateral HC junctions in both control and *Wls*^{cKO} OC (Fig. 3, m–p, arrows; Fig. 3 s). Finally, total protein levels of Fzd6 and Dvl2 were not significantly changed in *Wls*^{cKO} cochlear tissues, suggesting their delocalization was not due to loss of protein expression (Fig. 3, t and u). Thus, we conclude that Wnts regulate junctional localization of a subset of core PCP proteins.

To determine how Wnts regulate iPCP signaling, we examined the polarized distribution of representative iPCP effector proteins (Fig. S2). In addition to LGN and Gαi, which form a complex that localizes to the bare zone and lateral HC junctions, the PDZ-domain scaffold protein Par3 is asymmetrically localized along the lateral HC junctions. Par6 and aPKC are polarized on the medial side of the HC apical surface and junction. In *Wls*^{cKO} OC, laterally polarized distributions of LGN, Gαi, and Par3 were largely intact, albeit with mild misorientation matching the PCP defects (Fig. S2, b, d, and f). atypical protein kinase C (aPKC) was still medially polarized; however, staining intensity along the medial HC junctions was reduced (Fig. S2, g and h). These results suggest that planar polarized localization of iPCP proteins is largely independent of Wnt signaling.

Wnts regulate Daple localization and Gαi activity

Because junctional localization of Dvl2 was lost in *Wls*^{cKO} OC, we reasoned that Wnts may regulate a Dvl2-dependent process to mediate iPCP. As Daple is enriched along the lateral HC junctions where it interacts with both Gαi and Dvl2 (Siletti et al., 2017), we

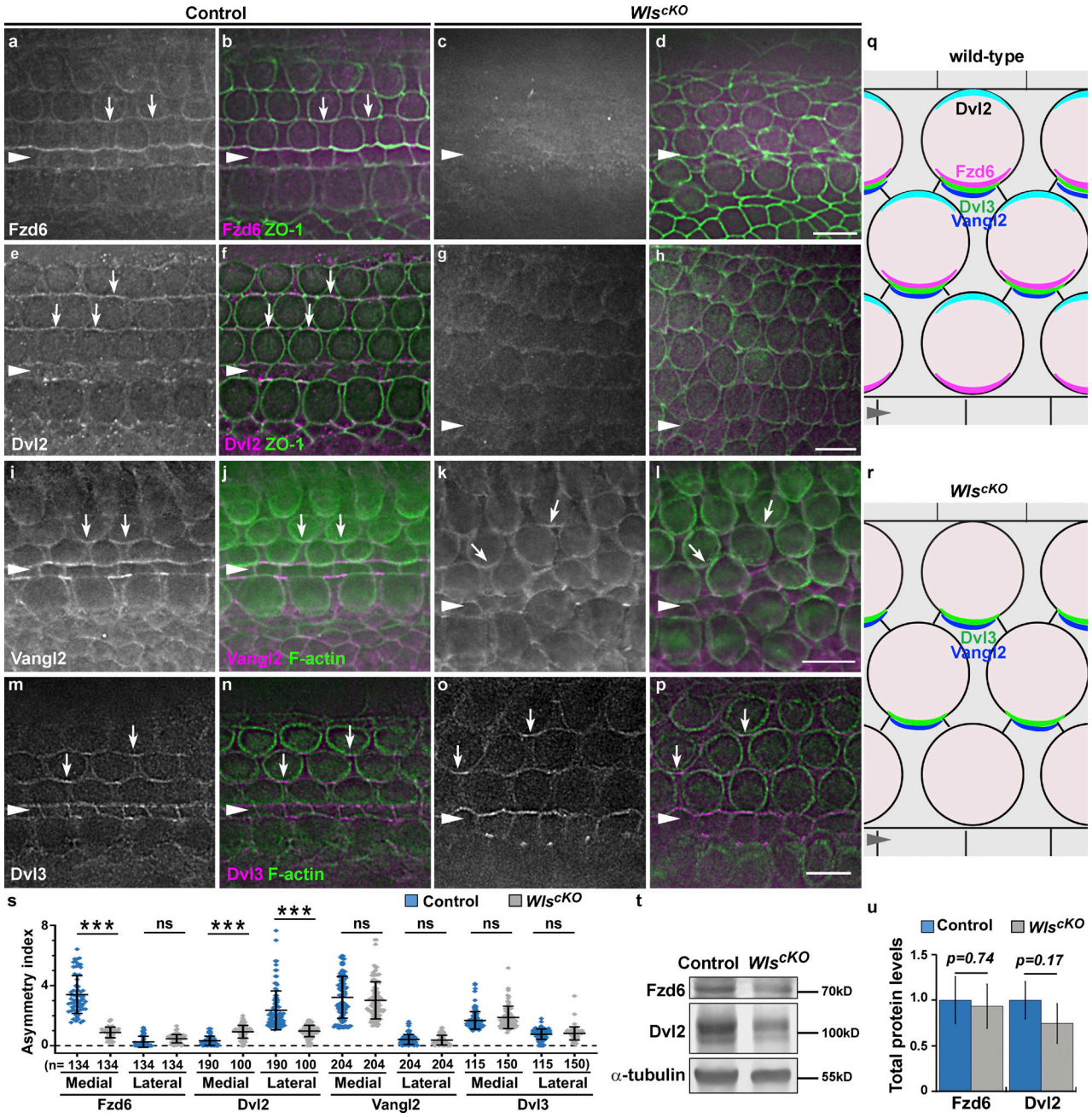

Figure 3. **Core PCP protein localization in *Wls*^{cKO} OC. (a–p)** Fzd6 (a–d), Dvl2 (e–h), Vangl2 (i–l), and Dvl3 (m–p) localization in the control and *Wls*^{cKO} OC at E18.5. Cell junctions were marked by ZO-1 or phalloidin staining. Scale bars, 6 µm. **(q and r)** Schematic diagrams of core PCP protein localization in control (p) and *Wls*^{cKO} OC (r). **(s)** Quantifications of PCP protein localization along the medial and lateral junctions of OHCs at E18.5. ***, P < 0.001; ns, not significant. **(t and u)** Western blot analysis of pooled E18.5 cochlear lysates probed with indicated antibodies (t) and protein level quantifications (u).

asked whether Wnts regulate Daple localization in the OC. In the control, Daple was enriched along the lateral HC junctions and in a punctate ring-like pattern around the HC basal body (Fig. 4, a, a', and c, arrows). Strikingly, in *Wls*^{cKO} OC, Daple localization at both subcellular locations was greatly reduced (Fig. 4, b, d, p, and q). Thus, Wnt signaling regulates Daple localization in the OC.

Disrupted localization of the Gαi GEF Daple in *Wls*^{cKO} OC suggested that Wnts regulate Gαi activation via Daple. To test this, we used antibodies specific to Gαi-GTP (Lane et al., 2008) to immunolocalize activated Gαi proteins. In the control, activated Gαi was detected in the HC apical cytoplasm and enriched in the kinocilium (Fig. 4, e and g, arrows; Fig. S3, a and b). In *Wls*^{cKO} OC, localization of Gαi-GTP to the kinocilium and apical cytoplasm was significantly reduced (Fig. 4, f and r). Together, these data reveal a role of Wnts in stimulating Gαi activity in the OC.

Inhibition of Gβγ led to PCP and iPCP defects

Inhibition of Gαi activity by pertussis toxin, which traps the G protein in the heterotrimeric complex, was shown to disrupt iPCP, indicating a requirement of Gαi proteins in iPCP (Ezan

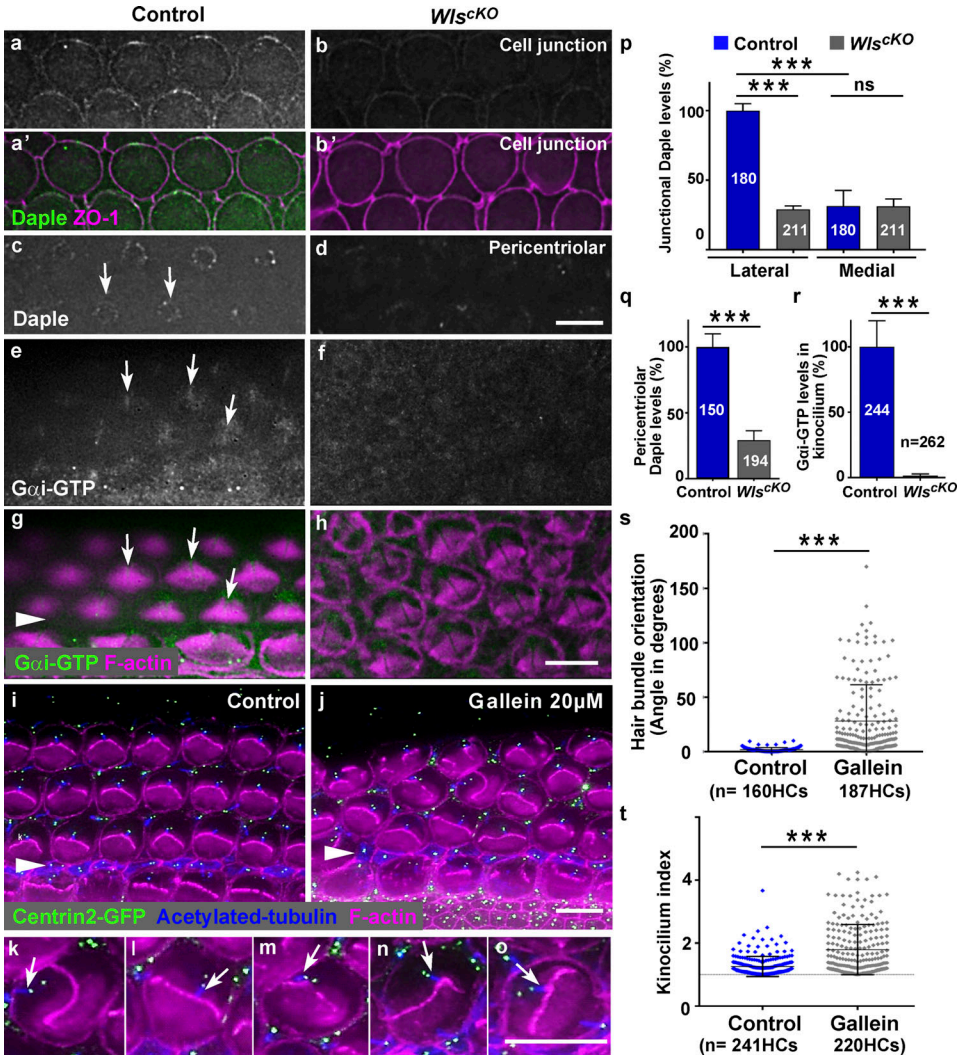

Figure 4. **Wnt-dependent G protein signaling regulates PCP in the OC. (a–d)** Daple localization to HC junctions (a–b') and around the basal body (c and d) in E18.5 control and *Wls*^{cKO} cochleae. **(e–h)** At E18.5, activated Gαi was enriched in the kinocilium in the control and greatly reduced in *Wls*^{cKO} OC (f and h). **(i–o)** Vehicle (i) or Gallein-treated cochlear explants (j–o) stained for F-actin (magenta), acetylated tubulin (blue), and GFP-Centrin2 (green). Scale bars, 6 µm. **(p–t)** Quantifications of Daple levels at HC junctions (p) and around the basal body (q), Gαi-GTP levels in the kinocilium (r), hair bundle orientation (s), and kinocilium positioning (t). ***, P < 0.001.

et al., 2013; Tarchini et al., 2013). However, whether the Gβγ heterodimer also plays a role in iPCP in the OC is unknown. To test this, we treated cochlear explants with Gallein, a Gβγ inhibitor that specifically blocks Gβγ-effector interactions without affecting the heterotrimeric G protein cycle (Lehmann et al., 2008; Lin and Smrcka, 2011). While HC polarity in control explants was largely normal (Fig.4 i), many HCs in Gallein-treated explants had misoriented and fragmented/misshapen hair bundles accompanied by a detached or aberrantly positioned kinocilium (Fig. 4, j–o, arrows). Furthermore, alignment of the HC centrioles along the medial-lateral axis (see Fig. 1 a') was defective as revealed by a GFP-Centrin2 transgene (Fig. 4, k–o). Thus, we conclude that Gβγ signaling is required for iPCP and PCP in the OC.

Wnts coordinate PCP and iPCP through phosphoinositide 3-kinase (PI3K)

Gβγ heterodimer can directly activate PI3Kγ (Brock et al., 2003). Moreover, Wnt5a can activate PI3K signaling in vitro in a Gβγ-dependent manner (Aznar et al., 2015). We therefore tested whether PI3K is a key effector of Wnt/G protein signaling in the cochlea. To assess PI3K signaling activity, we examined the localization of active AKT using antibodies against phospho-S473 AKT (pAKT). In the control at E18.5, pAKT was diffusely localized in the HC apical cytoplasm and enriched in the kinocilium (Fig. 5, a and b, arrows). In *Wls*^{cKO} OC, pAKT staining in the kinocilium was greatly reduced (Fig. 5, c, d, and i), suggesting that Wnts positively regulate PI3K signaling in HCs.

If PI3K is a crucial Wnt effector for HC polarity, then expression of a constitutively active form of PI3K should rescue PCP defects caused by *Wls* deletion. To this end, we generated *Wls*^{cKO}*; iPI3Kca/+* compound mutants expressing a Cre-inducible, constitutively active p110α catalytic subunit of PI3K (Adams et al., 2011). Embryos expressing iPI3Kca had an enlarged brain or exencephaly due to brain overgrowth, indicating effective iPI3Kca induction by *Emx2*^{Cre} (Fig. S3, c and d). Moreover, iPI3Kca induction did not interfere with *Wls* deletion as confirmed

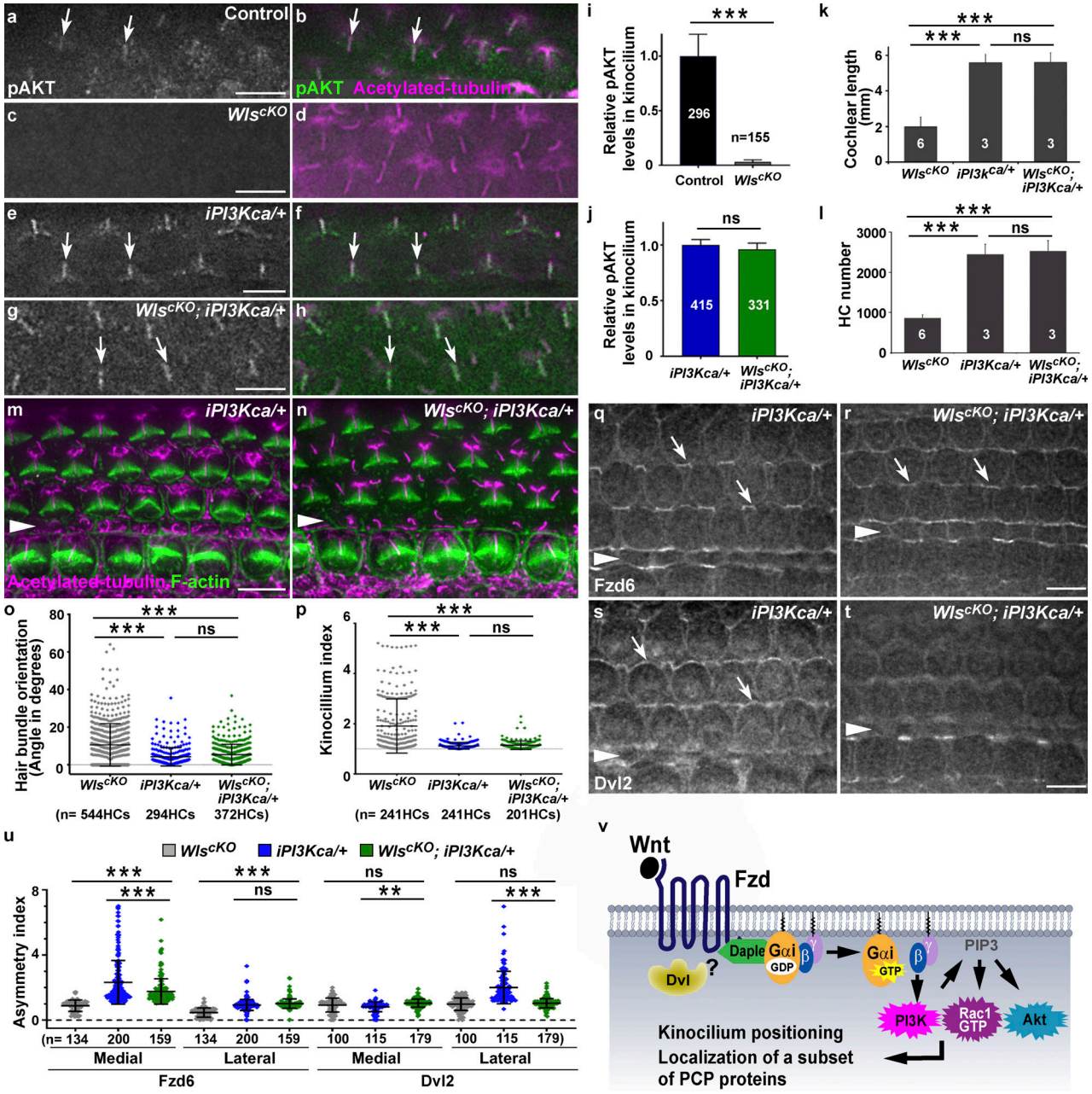

Figure 5. **Wnts signal through PI3K to coordinate iPCP and PCP in the OC. (a–h)** pAKT (green) and acetylated tubulin staining (magenta) in the control (a and b), *Wls*^{cKO} (c and d), *iPI3Kca/+* (e and f), and *Wls*^{cKO}*; iPI3Kca/+* OC (g and h) at E18.5. Arrows indicate the kinocilium. **(i–l)** Quantifications of pAKT levels in the kinocilium (i and j), cochlear length (k), and HC number (l). **(m and n)** E18.5 *iPI3Kca/+* (m) and *Wls*^{cKO}*; iPI3Kca/+* OC (n) stained for acetylated tubulin (magenta) and F-actin (green). **(o and p)** Quantifications of hair bundle orientation (o) and kinocilium positioning (p). **(q–t)** Fzd6 and Dvl2 localization in E18.5 *iPI3Kca/+* (q and s) and *Wls*^{cKO}*; iPI3Kca/+* OC (r and t). **(u)** Quantifications of Fzd6 and Dvl2 junctional localization. ***, P < 0.001; **, P < 0.01; ns, not significant. **(v)** A proposed Wnt/G protein/PI3K pathway for cochlear PCP regulation. Scale bars, 6 µm.

by Wls immunostaining at E16.5 (Fig. S3, e–h). In contrast to overgrowth of the brain, PI3Kca expression in the cochlea did not have any overt effect on OC cellular patterning, iPCP, or PCP (Fig. 5 m and Fig. S3 i). Neither did it affect pAKT localization to the kinocilium (Fig. 5, e and f). Importantly, pAKT localization to the kinocilium in *Wls*^{cKO}*; iPI3Kca/+* cochleae was restored to similar levels compared with *iPI3Kca/+* cochleae (Fig. 5, g, h, and j). Remarkably, iPI3Kca expression significantly rescued *Wls*^{cKO} cochlear defects, including cochlear length, HC numbers, hair bundle orientation, and kinocilium positioning (Fig. 5, k–p; and Fig. S3 j). We further examined Fzd6 and Dvl2 localization in the rescued cochleae. Interestingly, iPI3Kca expression significantly restored asymmetric localization of Fzd6, but not Dvl2 (Fig. 5, q–t, arrows; Fig. 5 u), suggesting that Dvl2 is genetically upstream of or in parallel with PI3K, which acts upstream of Fzd6. Together, these results indicate that PI3K is a key downstream effector of Wnt signaling that mediates both cochlear outgrowth and HC polarity in the cochlea.

Consistent with published studies (Aznar et al., 2015), our findings suggest a model in which Wnts activate Gαi proteins through membrane recruitment of Daple. In turn, free Gβγ activates PI3K to couple kinocilium positioning with hair bundle orientation and to localize a subset of core PCP proteins, thereby coordinating iPCP and PCP in the OC (Fig. 5 v). The putative Wnt/G protein/PI3K pathway likely plays a permissive role in HC polarity, as constitutive activation of PI3K signaling did not repolarize HCs or alter PCP vectors. The enrichment of active Gαi and AKT in the kinocilium raises the possibility that G protein–PI3K signaling acts within the kinocilium to maintain its position at the hair bundle vertex.

Previous studies suggest that canonical Wnt signaling within the cochlea promotes cell proliferation of otic precursors and radial patterning of medial-lateral compartments, and somewhat controversially, HC differentiation (Jacques et al., 2012; Jansson et al., 2019; Munnamalai and Fekete, 2016; Shi et al., 2014). Our study indicates that Wnts secreted from the cochlear epithelium are required for normal cochlear growth, but dispensable for HC differentiation. The medial and lateral compartments as demarcated by the pillar cell row were largely intact in Wls^{cKO} cochleae, consistent with the notion that Wnts cooperate with other morphogens to control radial patterning (Munnamalai and Fekete, 2016). Interestingly, the spiral ganglion was smaller in size and positioned abnormally in the absence of epithelial Wnts (Fig. 1 e), suggesting a codependence of neural and sensory patterning in the cochlea (Bok et al., 2013). PI3K inhibition has been previously shown to impair cochlear growth (Okano et al., 2011). Rescue of cochlear length and HC numbers in Wls^{cKO} cochleae by PI3K activation suggests that PI3K acts downstream of or in parallel with canonical Wnt signaling to promote otic precursor cell proliferation. The interplay between canonical Wnt and Wnt/G protein signaling in otic precursor cells remains to be determined.

We show that epithelial Wnts are required for asymmetric localization of Fzd6 and Dvl2, but not Vangl2 or Dvl3 in the OC. Similar results are independently reported (Huarcaya-Najarro et al., 2020). Together, these findings reveal a "fail-safe" mechanism to ensure robust generation of PCP vectors. In contrast to Wls^{cKO}, Daple knockout mice had normal cochlear length and Fz6 localization (Siletti et al., 2017), suggesting that additional GEFs are involved in Wnt/G protein signaling in the OC. Rescue of Fzd6 localization in Wls^{cKO} OC by PI3K activation suggests that Wnt/G protein signaling modulates the cortical cytoskeleton or the expression of as-yet unidentified factor(s) required for membrane trafficking and localization of Fzd6. Of note, the largely intact Vangl2 localization in the Wls^{cKO} cochlea contrasts with studies in the mouse limb mesenchyme and the *Xenopus* neural plate, where Wnt5a/Wnt11 regulate Vangl2 phosphorylation and asymmetric membrane localization (Gao et al., 2011; Ossipova et al., 2015). It is possible that Wnts from a non-epithelial source act redundantly to regulate Vangl2 localization. Alternatively, Vangl2 localization may be redundantly regulated by tissue mechanical forces, as observed in *Xenopus* larval skin (Chien et al., 2015).

The ligands and receptors for Wnt/G protein signaling in the OC remain to be identified. $Wnt5a^{-/-}$ mice had milder cochlear PCP defects than Wls^{cKO} mutants (Qian et al., 2007), suggesting additional Wnts are involved. Fdz7 and the closely related Fzd2 are candidate receptors: both are expressed in the developing OC; Fzd2 knockout mice have mild hair bundle orientation defects (Yu et al., 2010, 2012), while *fzd7a/b* was recently shown to regulate HC PCP in the zebrafish lateral line in parallel with *vangl2* (Navajas Acedo et al., 2019). The Wnt coreceptors Ror2 and Ptk7 have been implicated in PCP but not iPCP in the OC (Andreeva et al., 2014; Yamamoto et al., 2008), and therefore may have very minor, if any, involvement in Wnt/G protein signaling. Of note, PI3K activation did not restore Dvl2 localization in Wls^{cKO} cochleae, suggesting that, in addition to being a core PCP protein, Dvl2 may also mediate Wnt/G protein signaling. Future studies will shed light on the Wnt/G protein pathway components in the OC.

Materials and methods

Mice

Conditional deletion of *Wls* was achieved using a Wls^{flox} allele (Fu et al., 2011) and $Emx2^{Cre}$, which drives Cre expression in the cochlear epithelium starting from E12.5 (Kimura et al., 2005; Ono et al., 2014). Specifically, $Emx2^{Cre/+}$; $Wls^{flox/+}$ males were mated with $Wls^{flox/flox}$ or $Wls^{flox/+}$ females carrying the *R26-PI3Kca*H1047R* transgene (Jackson Laboratories, 16977). Rosa-mT/mG, Arl13b-mCherry, and GFP-Centrin2 transgenic mice (Bangs et al., 2015; Higginbotham et al., 2004; Muzumdar et al., 2007) were obtained from the Jackson Laboratories (007576, 027967, and 008234, respectively). Animal care and use were performed in compliance with National Institutes of Health guidelines and the Animal Care and Use Committee at the University of Virginia. For timed pregnancies, the morning of the plug was designated as E0.5, and the day of birth postnatal day 0 (P0).

Paint-fill and immunohistochemistry

Paint-fill analyses were performed as described previously (Grimsley-Myers et al., 2012). For immunostaining, temporal bones were fixed in 2 or 4% paraformaldehyde for 1 h at RT or in 10% TCA for 1 h on ice (indicated in the list in Table 1), then washed in PBS/glycine. Staining of whole-mount and cochlear cryo-sections was performed as previously described (Landin Malt et al., 2019). Briefly, cochlear sections or dissected cochleae were incubated in PBS containing 0.1% Triton X-100, 5% heat-inactivated goat/horse serum, and 0.02% NaN_3 for 1 h at RT, followed by overnight incubation with primary antibodies at 4°C. After three washes, samples were incubated with secondary antibodies and phalloidin/Hoechst 33342, post-fixed and washed, and mounted in Mowiol with 5% N-propyl gallate. Table 1 lists the antibodies used.

Microscopy and image analysis

Control and mutant samples were imaged under identical conditions. Images were collected at RT on a Deltavision deconvolution microscope with SoftWoRx software (Applied Precision), using an Olympus PlanApo 60×/1.42 NA oil-immersion objective, and Photometrics Cool Snap HQ2 camera, or on an Olympus

Table 1. **List of antibodies used**

Antibody	Concentration	Vendor	Catalog no.
Alexa-conjugated phalloidin	1:200	Thermo Fisher Scientific	A12379, A12380, A12381, A22287
Alexa-conjugated secondary antibodies	1:500	Thermo Fisher Scientific	A11036, A11029, A11057, A11077
Anti-acetylated tubulin	1:1,000	Sigma-Aldrich	T6793
Anti-aPKC	1:100	Santa Cruz	sc-216
Anti-Dvl2	1:100 (TCA)	Proteintech	12037-1-AP
Anti-Dvl3	1:200	Proteintech	13444-1-AP
Anti-Daple	1:400 (TCA)	Bethyl Laboratories	A302-951A
Anti-Fzd6	1:100 (TCA)	R & D Systems	AF1526-SP
Anti-Gαi3	1:500	Genetex	GTX14246
Anti-Gαi-GTP	1:100	NewEast Biociences	26901
Anti-GFP	1:500	Aveslab	GFP-1020
Anti-LGN	1:500	Homemade	Zheng et al., 2010
Anti-myosin VIIa	1:500	Proteus BioSciences	25-6790
Anti-Par3	1:500	Millipore	07-330
Anti-Par6	1:100	Santa Cruz	sc-166405
Anti-pS473-AKT	1:100	Cell Signaling	9271S
Anti-Sox2	1:500	Santa Cruz	sc-365823
Anti-Tuj1	1:500	Biolegend	MMS-435P
Anti-Vangl2	1:100	Millipore	MABN750
Anti-Wls	1:600	Kerafast	EUR302
Anti-ZO-1	1:200 (TCA)	DSHB	R26.4C-c
Hoechst 33342	1:10,000	Thermo Fisher Scientific	H3570

FV1000 confocal microscope with photomultiplier tube detectors and Fluoview software, using an Olympus UPlanSApo 60×/1.35 NA oil-immersion objective. Image processing, including adjustments of brightness, contrast, and gamma level, were performed using Fiji (National Institutes of Health) and Photoshop (Adobe). All micrographs of the OC were shown with the lateral side up, and the row of inner pillar cells was indicated by an arrowhead.

Quantification of HC phenotypes

Cochlear length, HC number, hair bundle orientation, and kinocilium position were quantified as previously described (Landin Malt et al., 2019). For hair bundle orientation, a reference line was drawn parallel to the row of inner pillar cells, and another line connecting the two ends of the hair bundle. The angle formed by the two lines indicated bundle misorientation in degrees. For kinocilium positioning in relation to the hair bundle, the distances from the tip of the kinocilium to the ends of the hair bundle were measured, and their ratio (x/y, x ≥ y) was plotted as kinocilium index. Off-center kinocilium had an index value >1.5.

Quantification of protein localization

Immunostaining of various polarity proteins in the OHC region was quantified from single optic sections following background subtraction using Fiji. For core PCP proteins, apical cell junctions were identified by either ZO-1 or F-actin staining. Next, a 30 × 10–pixel region of interest (ROI) centered around the medial, lateral, or orthogonal HC junctions was selected. As such, the ROI contained the plasma membranes and cell cortex of the HC-SC pair. PCP protein staining intensity in the medial or lateral ROI was normalized to that of the orthogonal ROI of the same HC, and the ratio was plotted as "Asymmetry Index." Because strong staining in pillar cells often overlapped with medial junctions of OHC1, only OHC2 and OHC3 rows were quantified. For protein localization in the kinocilium, a 20 × 5–pixel ROI centered around the kinocilium was selected. Protein staining intensity in the ROI was normalized to the mean of the littermate control, and plotted as percentages of control levels. For Daple cortical localization, the staining intensity of the medial and lateral ROIs was plotted as percentages of the mean of control lateral ROIs. For Daple pericentriolar localization, a 33-pixel-diameter ROI around the basal body was selected, and staining intensity was plotted as percentages of the mean of control ROIs.

Western blot analysis

Cochleae were dissected from E18.5 Wls^{cKO} and littermate controls. Following extraction in lysis buffer (1% Triton X-100, 20 mM Hepes, pH 7.4, 0.14 M NaCl, 5% glycerol, 1 mM vanadate, 25 mM NaF, protease and phosphatase inhibitors), pooled lysates of 6 Wls^{cKO} or four control cochleae were loaded into one well.

For Western blot analysis, membranes were incubated with primary antibodies (Fzd6, Abclonal A10503, 1:1,000; Dvl2, Proteintech 12037–1-AP, 1:2,000; and α-tubulin, Sigma-Aldrich T6074, 1:10,000), followed by appropriate LI-COR IRDye secondary antibodies, and visualized using the Li-COR Odyssey CLx Imaging System. Quantifications were calculated with LI-COR Image Studio Software.

Statistical analysis

A minimum of three independent experiments was analyzed for all quantifications. The numbers of individual data points were indicated in the figures or figure legends. All data were presented as mean ± SD. Significance was tested using a two-tailed Student's *t* test or one-way ANOVA followed by a Tukey's multiple comparison test (GraphPad Prism).

Scanning electron microscopy

Temporal bones were fixed at RT for 1 h in 0.1 M sodium cacodylate buffer containing 4% formaldehyde, 2.5% glutaraldehyde, 10 mM $CaCl_2$, and 5 mM $MgCl_2$. Cochleae were then dissected and postfixed overnight at 4°C. Cochleae were washed and then dehydrated in a series of graded ethanol washes, dried overnight in hexamethyldisilazane (Electron Microscopy Science 16700), mounted on metal stubs, and sputter coated with 5 nm gold. Samples were imaged on a Zeiss Sigma VP HD field emission scanning electron microscope at 30 kV.

Cochlear explants

E15.5 cochleae were dissected and the Reissner's membranes removed to expose the sensory epithelium. Explants were cultured in DMEM/F12 containing N2 Supplement and ampicillin in Lab-Tek chamber slides (C6932) precoated with CellTak (Thermo Fisher Scientific, CB40240). After overnight incubation at 37°C 5% CO_2, explants were treated with 20 µM Gallein (Tocris Bioscience, 3090) or DMSO as vehicle control. Media were replaced daily, and cochleae were fixed after 4 d in vitro, immunostained, and imaged as previously described (Andreeva et al., 2014).

Skeletal preparation

Skinned and eviscerated E18.5 embryos were fixed in 100% ethanol for 24 h followed by 100% acetone for 24 h, then stained in Alcian Blue/Alizarin Red for 4 d at 37°C. Embryos were washed in 1% KOH until the staining appeared optimal and cleared through a 1% KOH/glycerol series.

Online supplemental material

Fig. S1 (related to Fig. 1) shows gross phenotypes of Wls^{cKO} embryos; Fig. S2 (related to Fig. 3) shows localizations of representative iPCP proteins; and Fig. S3 (related to Fig. 5) includes controls confirming *iPI3Kca* induction and *Wls* deletion.

Acknowledgments

We thank Drs. Quansheng Du (Augusta University, Augusta, GA) and Ann Sutherland (University of Virginia, Charlottesville, VA) for reagents, Dr. Doris Wu (National Institutes of Health, Bethesda, MD) for advice on the paint-fill technique, Drs. Alan Cheng and Elvis Huarcaya Najarro for helpful discussions (Stanford University, Palo Alto, CA), Wenxia Li for technical assistance, and Shaylyn Clancy and Drs. Bettina Winckler, James Casanova, and Jung-bum Shin for critical reading of the manuscript.

This study was supported by National Institutes of Health grant R01DC013773 (to X. Lu).

The authors declare no competing interests.

Author contributions: A. Landin Malt and X. Lu designed research, performed experiments, analyzed data, and wrote the paper; A. Hogan, C. Smith, and M. Madani performed experiments and analyzed data.

Submitted: 12 December 2019
Revised: 15 April 2020
Accepted: 13 July 2020

References

Adams, J.R., K. Xu, J.C. Liu, N.M. Agamez, A.J. Loch, R.G. Wong, W. Wang, K.L. Wright, T.F. Lane, E. Zacksenhaus, et al. 2011. Cooperation between Pik3ca and p53 mutations in mouse mammary tumor formation. *Cancer Res.* 71:2706–2717. https://doi.org/10.1158/0008-5472.CAN-10-0738

Andreeva, A., J. Lee, M. Lohia, X. Wu, I.G. Macara, and X. Lu. 2014. PTK7-Src signaling at epithelial cell contacts mediates spatial organization of actomyosin and planar cell polarity. *Dev. Cell.* 29:20–33. https://doi.org/10.1016/j.devcel.2014.02.008

Aw, W.Y., and D. Devenport. 2017. Planar cell polarity: global inputs establishing cellular asymmetry. *Curr. Opin. Cell Biol.* 44:110–116. https://doi.org/10.1016/j.ceb.2016.08.002

Aznar, N., K.K. Midde, Y. Dunkel, I. Lopez-Sanchez, Y. Pavlova, A. Marivin, J. Barbazán, F. Murray, U. Nitsche, K.-P. Janssen, et al. 2015. Daple is a novel non-receptor GEF required for trimeric G protein activation in Wnt signaling. *eLife.* 4. e07091. https://doi.org/10.7554/eLife.07091

Bangs, F.K., N. Schrode, A.K. Hadjantonakis, and K.V. Anderson. 2015. Lineage specificity of primary cilia in the mouse embryo. *Nat. Cell Biol.* 17:113–122. https://doi.org/10.1038/ncb3091

Bänziger, C., D. Soldini, C. Schütt, P. Zipperlen, G. Hausmann, and K. Basler. 2006. Wntless, a conserved membrane protein dedicated to the secretion of Wnt proteins from signaling cells. *Cell.* 125:509–522. https://doi.org/10.1016/j.cell.2006.02.049

Bartscherer, K., N. Pelte, D. Ingelfinger, and M. Boutros. 2006. Secretion of Wnt ligands requires Evi, a conserved transmembrane protein. *Cell.* 125:523–533. https://doi.org/10.1016/j.cell.2006.04.009

Beer-Hammer, S., S.C. Lee, S.A. Mauriac, V. Leiss, I.A.M. Groh, A. Novakovic, R.P. Piekorz, K. Bucher, C. Chen, K. Ni, et al. 2018. Gαi Proteins are Indispensable for Hearing. *Cell. Physiol. Biochem.* 47:1509–1532. https://doi.org/10.1159/000490867

Bok, J., C. Zenczak, C.H. Hwang, and D.K. Wu. 2013. Auditory ganglion source of Sonic hedgehog regulates timing of cell cycle exit and differentiation of mammalian cochlear hair cells. *Proc. Natl. Acad. Sci. USA.* 110:13869–13874. https://doi.org/10.1073/pnas.1222341110

Brock, C., M. Schaefer, H.P. Reusch, C. Czupalla, M. Michalke, K. Spicher, G. Schultz, and B. Nürnberg. 2003. Roles of G beta gamma in membrane recruitment and activation of p110 gamma/p101 phosphoinositide 3-kinase gamma. *J. Cell Biol.* 160:89–99. https://doi.org/10.1083/jcb.200210115

Butler, M.T., and J.B. Wallingford. 2017. Planar cell polarity in development and disease. *Nat. Rev. Mol. Cell Biol.* 18:375–388. https://doi.org/10.1038/nrm.2017.11

Chien, Y.H., R. Keller, C. Kintner, and D.R. Shook. 2015. Mechanical strain determines the axis of planar polarity in ciliated epithelia. *Curr. Biol.* 25:2774–2784. https://doi.org/10.1016/j.cub.2015.09.015

Etheridge, S.L., S. Ray, S. Li, N.S. Hamblet, N. Lijam, M. Tsang, J. Greer, N. Kardos, J. Wang, D.J. Sussman, et al. 2008. Murine dishevelled 3 functions in redundant pathways with dishevelled 1 and 2 in normal cardiac outflow tract, cochlea, and neural tube development. *PLoS Genet.* 4. e1000259. https://doi.org/10.1371/journal.pgen.1000259

Ezan, J., L. Lasvaux, A. Gezer, A. Novakovic, H. May-Simera, E. Belotti, A.C. Lhoumeau, L. Birnbaumer, S. Beer-Hammer, J.P. Borg, et al. 2013. Primary cilium migration depends on G-protein signalling control of subapical cytoskeleton. *Nat. Cell Biol.* 15:1107–1115. https://doi.org/10.1038/ncb2819

Fu, J., H.M. Ivy Yu, T. Maruyama, A.J. Mirando, and W. Hsu. 2011. Gpr177/mouse Wntless is essential for Wnt-mediated craniofacial and brain development. *Dev. Dyn.* 240:365–371. https://doi.org/10.1002/dvdy.22541

Gao, B., H. Song, K. Bishop, G. Elliot, L. Garrett, M.A. English, P. Andre, J. Robinson, R. Sood, Y. Minami, et al. 2011. Wnt signaling gradients establish planar cell polarity by inducing Vangl2 phosphorylation through Ror2. *Dev. Cell.* 20:163–176. https://doi.org/10.1016/j.devcel.2011.01.001

Grimsley-Myers, C.M., C.W. Sipe, G.S. Géléoc, and X. Lu. 2009. The small GTPase Rac1 regulates auditory hair cell morphogenesis. *J. Neurosci.* 29:15859–15869. https://doi.org/10.1523/JNEUROSCI.3998-09.2009

Grimsley-Myers, C.M., C.W. Sipe, D.K. Wu, and X. Lu. 2012. Redundant functions of Rac GTPases in inner ear morphogenesis. *Dev. Biol.* 362:172–186. https://doi.org/10.1016/j.ydbio.2011.12.008

Higginbotham, H., S. Bielas, T. Tanaka, and J.G. Gleeson. 2004. Transgenic mouse line with green-fluorescent protein-labeled Centrin 2 allows visualization of the centrosome in living cells. *Transgenic Res.* 13:155–164. https://doi.org/10.1023/B:TRAG.0000026071.41735.8e

Huarcaya-Najarro, E., J. Huang, L. Quiruz, A. Jacobo, N. Grillet, and A.G. Cheng. 2020. Dual regulation of planar polarization by Wnt secretion and Vangl2 in the developing mouse cochlea. *Development*. https://doi.org/10.1242/dev.191981

Ishida-Takagishi, M., A. Enomoto, N. Asai, K. Ushida, T. Watanabe, T. Hashimoto, T. Kato, L. Weng, S. Matsumoto, M. Asai, et al. 2012. The Dishevelled-associating protein Daple controls the non-canonical Wnt/Rac pathway and cell motility. *Nat. Commun.* 3:859. https://doi.org/10.1038/ncomms1861

Jacques, B.E., C. Puligilla, R.M. Weichert, A. Ferrer-Vaquer, A.-K. Hadjantonakis, M.W. Kelley, and A. Dabdoub. 2012. A dual function for canonical Wnt/β-catenin signaling in the developing mammalian cochlea. *Development*. 139:4395–4404. https://doi.org/10.1242/dev.080358

Jansson, L., M. Ebeid, J.W. Shen, T.E. Mokhtari, L.A. Quiruz, D.M. Ornitz, S.-H. Huh, and A.G. Cheng. 2019. β-Catenin is required for radial cell patterning and identity in the developing mouse cochlea. *Proc. Natl. Acad. Sci. USA*. 116:21054–21060. https://doi.org/10.1073/pnas.1910223116

Kimura, J., Y. Suda, D. Kurokawa, Z.M. Hossain, M. Nakamura, M. Takahashi, A. Hara, and S. Aizawa. 2005. Emx2 and Pax6 function in cooperation with Otx2 and Otx1 to develop caudal forebrain primordium that includes future archipallium. *J. Neurosci.* 25:5097–5108. https://doi.org/10.1523/JNEUROSCI.0239-05.2005

Kirjavainen, A., M. Laos, T. Anttonen, and U. Pirvola. 2015. The Rho GTPase Cdc42 regulates hair cell planar polarity and cellular patterning in the developing cochlea. *Biol. Open.* 4:516–526. https://doi.org/10.1242/bio.20149753

Landin Malt, A., Z. Dailey, J. Holbrook-Rasmussen, Y. Zheng, A. Hogan, Q. Du, and X. Lu. 2019. Par3 is essential for the establishment of planar cell polarity of inner ear hair cells. *Proc. Natl. Acad. Sci. USA*. 116:4999–5008. https://doi.org/10.1073/pnas.1816333116

Lane, J.R., D. Henderson, B. Powney, A. Wise, S. Rees, D. Daniels, C. Plumpton, I. Kinghorn, and G. Milligan. 2008. Antibodies that identify only the active conformation of G(i) family G protein alpha subunits. *FASEB J.* 22:1924–1932. https://doi.org/10.1096/fj.07-100388

Lehmann, D.M., A.M. Seneviratne, and A.V. Smrcka. 2008. Small molecule disruption of G protein beta gamma subunit signaling inhibits neutrophil chemotaxis and inflammation. *Mol. Pharmacol.* 73:410–418. https://doi.org/10.1124/mol.107.041780

Lin, Y., and A.V. Smrcka. 2011. Understanding molecular recognition by G protein βγ subunits on the path to pharmacological targeting. *Mol. Pharmacol.* 80:551–557. https://doi.org/10.1124/mol.111.073072

Montcouquiol, M., R.A. Rachel, P.J. Lanford, N.G. Copeland, N.A. Jenkins, and M.W. Kelley. 2003. Identification of Vangl2 and Scrb1 as planar polarity genes in mammals. *Nature*. 423:173–177. https://doi.org/10.1038/nature01618

Montcouquiol, M., N. Sans, D. Huss, J. Kach, J.D. Dickman, A. Forge, R.A. Rachel, N.G. Copeland, N.A. Jenkins, D. Bogani, et al. 2006. Asymmetric localization of Vangl2 and Fz3 indicate novel mechanisms for planar cell polarity in mammals. *J. Neurosci.* 26:5265–5275. https://doi.org/10.1523/JNEUROSCI.4680-05.2006

Munnamalai, V., and D.M. Fekete. 2016. Notch-Wnt-Bmp crosstalk regulates radial patterning in the mouse cochlea in a spatiotemporal manner. *Development*. 143:4003–4015. https://doi.org/10.1242/dev.139469

Muzumdar, M.D., B. Tasic, K. Miyamichi, L. Li, and L. Luo. 2007. A global double-fluorescent Cre reporter mouse. *Genesis*. 45:593–605. https://doi.org/10.1002/dvg.20335

Navajas Acedo, J., M.G. Voas, R. Alexander, T. Woolley, J.R. Unruh, H. Li, C. Moens, and T. Piotrowski. 2019. PCP and Wnt pathway components act in parallel during zebrafish mechanosensory hair cell orientation. *Nat. Commun.* 10:3993. https://doi.org/10.1038/s41467-019-12005-y

Nichols, A.S., D.H. Floyd, S.P. Bruinsma, K. Narzinski, and T.J. Baranski. 2013. Frizzled receptors signal through G proteins. *Cell. Signal.* 25:1468–1475. https://doi.org/10.1016/j.cellsig.2013.03.009

Okano, T., S. Xuan, and M.W. Kelley. 2011. Insulin-like growth factor signaling regulates the timing of sensory cell differentiation in the mouse cochlea. *J. Neurosci.* 31:18104–18118. https://doi.org/10.1523/JNEUROSCI.3619-11.2011

Oldham, W.M., and H.E. Hamm. 2008. Heterotrimeric G protein activation by G-protein-coupled receptors. *Nat. Rev. Mol. Cell Biol.* 9:60–71. https://doi.org/10.1038/nrm2299

Ono, K., T. Kita, S. Sato, P. O'Neill, S.-S. Mak, M. Paschaki, M. Ito, N. Gotoh, K. Kawakami, Y. Sasai, et al. 2014. FGFR1-Frs2/3 signalling maintains sensory progenitors during inner ear hair cell formation. *PLoS Genet.* 10.e1004118. https://doi.org/10.1371/journal.pgen.1004118

Ossipova, O., K. Kim, and S.Y. Sokol. 2015. Planar polarization of Vangl2 in the vertebrate neural plate is controlled by Wnt and Myosin II signaling. *Biol. Open.* 4:722–730. https://doi.org/10.1242/bio.201511676

Qian, D., C. Jones, A. Rzadzinska, S. Mark, X. Zhang, K.P. Steel, X. Dai, and P. Chen. 2007. Wnt5a functions in planar cell polarity regulation in mice. *Dev. Biol.* 306:121–133. https://doi.org/10.1016/j.ydbio.2007.03.011

Scheffer, D.I., J. Shen, D.P. Corey, and Z.Y. Chen. 2015. Gene Expression by Mouse Inner Ear Hair Cells during Development. *J. Neurosci.* 35:6366–6380. https://doi.org/10.1523/JNEUROSCI.5126-14.2015

Schulte, G., and S.C. Wright. 2018. Frizzleds as GPCRs - More Conventional Than We Thought!. *Trends Pharmacol. Sci.* 39:828–842. https://doi.org/10.1016/j.tips.2018.07.001

Shi, F., L. Hu, B.E. Jacques, J.F. Mulvaney, A. Dabdoub, and A.S. Edge. 2014. β-Catenin is required for hair-cell differentiation in the cochlea. *J. Neurosci.* 34:6470–6479. https://doi.org/10.1523/JNEUROSCI.4305-13.2014

Siletti, K., B. Tarchini, and A.J. Hudspeth. 2017. Daple coordinates organ-wide and cell-intrinsic polarity to pattern inner-ear hair bundles. *Proc. Natl. Acad. Sci. USA*. 114:E11170–E11179. https://doi.org/10.1073/pnas.1716522115

Sipe, C.W., and X. Lu. 2011. Kif3a regulates planar polarization of auditory hair cells through both ciliary and non-ciliary mechanisms. *Development*. 138:3441–3449. https://doi.org/10.1242/dev.065961

Sipe, C.W., L. Liu, J. Lee, C. Grimsley-Myers, and X. Lu. 2013. Lis1 mediates planar polarity of auditory hair cells through regulation of microtubule organization. *Development*. 140:1785–1795. https://doi.org/10.1242/dev.089763

Song, H., J. Hu, W. Chen, G. Elliott, P. Andre, B. Gao, and Y. Yang. 2010. Planar cell polarity breaks bilateral symmetry by controlling ciliary positioning. *Nature*. 466:378–382. https://doi.org/10.1038/nature09129

Tarchini, B., and X. Lu. 2019. New insights into regulation and function of planar polarity in the inner ear. *Neurosci. Lett.* 709. 134373. https://doi.org/10.1016/j.neulet.2019.134373

Tarchini, B., C. Jolicoeur, and M. Cayouette. 2013. A molecular blueprint at the apical surface establishes planar asymmetry in cochlear hair cells. *Dev. Cell.* 27:88–102. https://doi.org/10.1016/j.devcel.2013.09.011

Wang, J., S. Mark, X. Zhang, D. Qian, S.J. Yoo, K. Radde-Gallwitz, Y. Zhang, X. Lin, A. Collazo, A. Wynshaw-Boris, et al. 2005. Regulation of polarized extension and planar cell polarity in the cochlea by the vertebrate PCP pathway. *Nat. Genet.* 37:980–985. https://doi.org/10.1038/ng1622

Wang, Y., N. Guo, and J. Nathans. 2006. The role of Frizzled3 and Frizzled6 in neural tube closure and in the planar polarity of inner-ear sensory hair cells. *J. Neurosci.* 26:2147–2156. https://doi.org/10.1523/JNEUROSCI.4698-05.2005

Yamamoto, S., O. Nishimura, K. Misaki, M. Nishita, Y. Minami, S. Yonemura, H. Tarui, and H. Sasaki. 2008. Cthrc1 selectively activates the planar cell polarity pathway of Wnt signaling by stabilizing the Wnt-receptor complex. *Dev. Cell.* 15:23–36. https://doi.org/10.1016/j.devcel.2008.05.007

Yang, Y., and M. Mlodzik. 2015. Wnt-Frizzled/planar cell polarity signaling: cellular orientation by facing the wind (Wnt). *Annu. Rev. Cell Dev. Biol.* 31:623–646. https://doi.org/10.1146/annurev-cellbio-100814-125315

Yu, H., P.M. Smallwood, Y. Wang, R. Vidaltamayo, R. Reed, and J. Nathans. 2010. Frizzled 1 and frizzled 2 genes function in palate, ventricular septum and neural tube closure: general implications for tissue fusion processes. *Development*. 137:3707–3717. https://doi.org/10.1242/dev.052001

Yu, H., X. Ye, N. Guo, and J. Nathans. 2012. Frizzled 2 and frizzled 7 function redundantly in convergent extension and closure of the ventricular septum and palate: evidence for a network of interacting genes. *Development*. 139:4383–4394. https://doi.org/10.1242/dev.083352

Zheng, Z., H. Zhu, Q. Wan, J. Liu, Z. Xiao, D.P. Siderovski, and Q. Du. 2010. LGN regulates mitotic spindle orientation during epithelial morphogenesis. *J. Cell Biol.* 189:275–288. https://doi.org/10.1083/jcb.200910021

Supplemental material

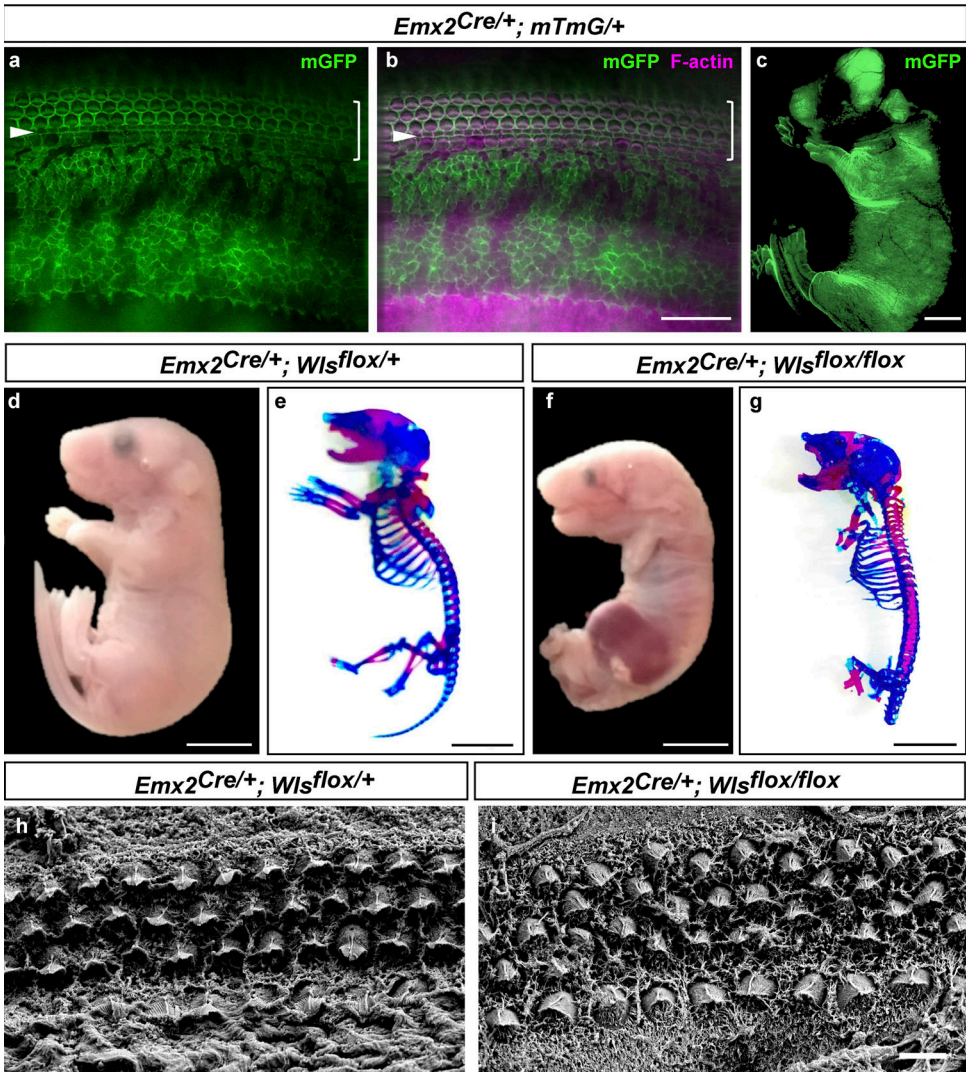

Figure S1. **Wls deletion in multiple tissues mediated by *Emx2*^{Cre}. (a–c)** Patterns of *Emx2*^{Cre}-mediated recombination as indicated by the Rosa-mT/mG reporter. Membrane GFP (mGFP, green) marked recombined cells in the cochlear epithelium (a and b) and other tissues in the mouse embryo (c) at P0. Magenta, phalloidin staining. **(d–g)** Gross developmental defects in *Wls*^{cKO} embryos at E18.5 (e and g). **(e and g)** Whole-mount skeletal staining using Alcian blue and Alizarin red to identify cartilage and bone, respectively. **(h and i)** Scanning electron micrographs of E18.5 control (h) and *Wls*^{cKO} OC (i). Scale bars: a and b, 50 µm; c–g, 6 mm; h and i, 4 µm.

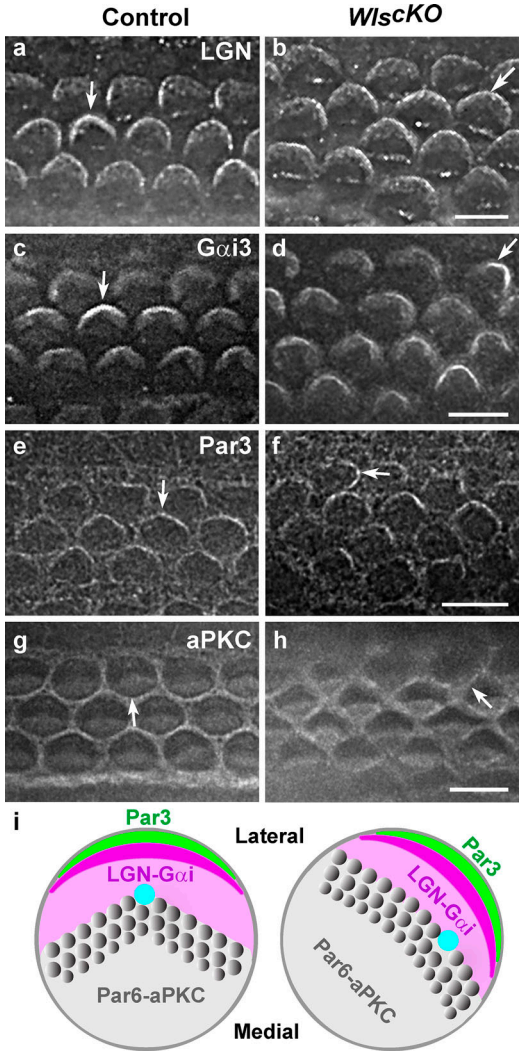

Figure S2. **Localization of iPCP proteins in *Wls*^{cKO} cochleae. (a–f)** Laterally polarized localization of LGN (a and b), Gαi3 (c and d), and Par3 (e and f) was maintained in *Wls*^{cKO} OC. **(g and h)** aPKC was still polarized to the medial HC apex. All stainings were performed at E18.5, except for Par3, which was at E17.5. Arrows indicate normal (a, c, e, and g) and misoriented iPCP protein localization (b, d, f, and h) relative to the medial-lateral axis. Only OHC rows were shown. **(i)** Schematic diagrams of iPCP protein localization in wild-type and *Wls*^{cKO} HCs. Lateral is up. Scale bars, 6 µm.

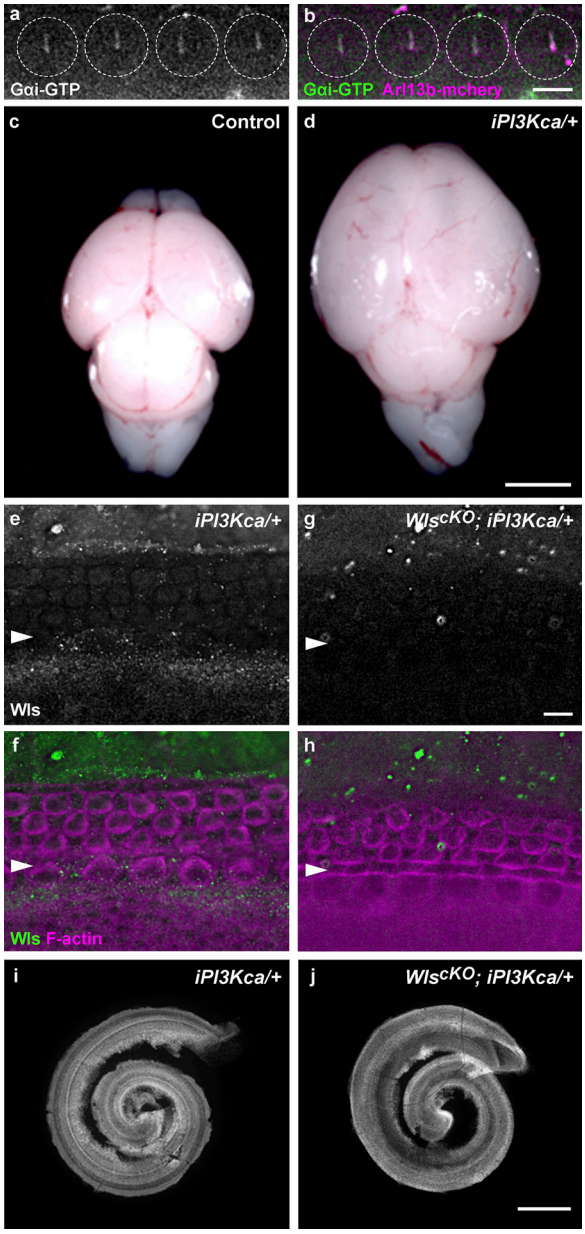

Figure S3. **Expression of constitutively active PI3Kca induced by *Emx2*^{Cre}. (a and b)** In P0 HCs (outlined), Gαi-GTP (green) is enriched in the kinocilium, which is marked by the ciliary marker Arl13b-mCherry (magenta). **(c and d)** *Emx2*^{Cre}-mediated expression of constitutively active PI3K resulted in enlarged brain (d). **(e–h)** E16.5 cochleae whole-mount stained for Wls (green). Wls expression in the OC and adjacent nonsensory epithelia was greatly reduced in *Wls*^{cKO}*; iPI3Kca/+* cochleae (g and h). Magenta, phalloidin staining. **(i and j)** E18.5 *iPI3Kca/+* (i) and *Wls*^{cKO}*; iPI3Kca/+* cochleae (j) had normal length. Scale bars: a and b, 6 µm; c and d, 1 mm; e–h, 6 µm; i and j, 100 µm.